JOURNAL OF COMPUTATIONAL PHYSICS 121, 115–128 (1995)

Material-Based Limiters for the Time-Domain Maxwell Equations with Thin Conducting Sheets

DAVID G. BISHOP

MDA Engineering, Inc., Arlington, Texas 76010

Received March 26, 1993; revised March 16, 1995

An explicit upwind-difference predictor–corrector integration scheme is applied to the time-domain Maxwell equations of electromagnetics using a cell-centered finite-volume implementation. The characteristic-based numerical flux and material-based limiters (which are scalar coefficients of the extended second-order correction terms in the corrector step) are reformulated for a material interface that contains a thin electric and-or thin magnetic conducting sheet. The integration scheme requires the material-based limiters to correctly model wave reflection and transmission at a material interface and to enable the numerical solution to be advanced at the maximum timestep prescribed by linear stability analysis. The effect of material-based limiters is demonstrated for one-dimensional wave propagation in isotropic nonhomogeneous materials with and without thin conducting sheets.

INTRODUCTION

An important objective of computational electromagnetics (CEM) is the ability to accurately predict the propagation of time-varying electromagnetic (EM) fields in constant-property homogeneous materials (free-space) and nonhomogeneous materials with regions of spatially varying electric and magnetic properties, which may contain thin electric and magnetic conducting sheets.

The time-accurate numerical methods developed in computational fluid dynamics (CFD) for solution of the Euler equations can be applied to solve the time-domain Maxwell equations of electromagnetics, both total-field and scattered-field formulations. With the CFD-based finite-volume (FV-TD) methods, the conservation-law volume-integral form of the time-domain Maxwell equations is implemented. For an upwind characteristic-based difference scheme, the electric and magnetic field vectors are integrated concurrently at the same grid-coordinate location in space and time. A distinction is made between the algorithm that is used to time integrate cell-averaged quantities (the electric and magnetic fields and material properties) and the scheme that is used to construct the numerical flux (the tangential vector component of the electric and magnetic fields) at the cell interface from this same cell-centered information.

A spatially structured geometric discretization of the computational domain defines the system of curvilinear grid-coordinates that conform to specified computational boundaries, such that regions with uniform material properties are bounded by constant grid-coordinate surfaces. With a cell-centered finite-volume implementation, the spatial variation of material properties is represented by cell-averaged values, which means that the interface between contiguous cells is a material interface across which the electric and magnetic material properties may be discontinuous. As shown in Fig. 1, the material interface can contain a thin electric and-or a thin magnetic conducting sheet that is a sub-grid material property coincident with a constant grid-coordinate surface. With no thin conducting sheet, the tangential vector component of the total electric and magnetic fields is continuous at the material interface. The tangential vector component of the total magnetic/electric field is discontinuous across a thin electric/magnetic conducting sheet, respectively.

For the numerical integration scheme, the first-order numerical flux and second-order extrapolation across consecutive cells (to obtain better than first-order spatial accuracy) must account for the effect on wave propagation of the change in material impedance across the cell interface. This must be done implicitly by construction within the numerical flux and explicitly in the predictor–corrector scheme by the addition of scalar coefficients, called material-based limiters, on the second-order terms in the corrector step.

For time-domain solution of the Maxwell equations, Shankar *et al.* [1–5] implemented the upwind-difference form of the Lax–Wendroff two-step integration scheme, which is the second-order predictor–corrector scheme that was developed by Warming and Beam [6]. The numerical flux was derived for the propagation of electromagnetic waves in linear isotropic nonhomogeneous materials with a spatially varying material impedance and thin electric conducting sheets. In terms of cell-averaged quantities and properties of the conducting sheet, the numerical flux was defined by a characteristic-based integration that is the exact solution of a one-dimensional Riemann problem, as prescribed by Lax [7] and Osher and Solomon [8]. For grid-aligned wave propagation in a region of constant material impedance and no thin conducting sheets, this method satisfies the perfect-shift condition at timesteps for which CFL = 1 and

0021-9991/95 $12.00

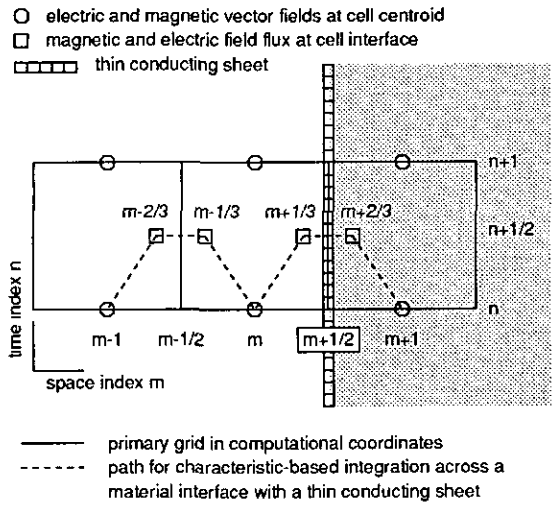

FIG. 1. Computational space-time network used for the CFD-based upwind-difference scheme in one dimension.

CFL = 2 in one dimension, which represents all integer CFL numbers for which the method is stable (the CFL number is the product of the wave speed and time step divided by the cell volume, in one dimension). With the constraint that the cell volume divided by the wave speed is equal to a constant, then the one-dimensional perfect-shift condition ensures that the integration scheme can reproduce the exact solution, with no numerically induced dissipation or dispersion.

In the research by Bishop and Anderson [9], the following enhancements to the upwind predictor–corrector scheme were developed for solution in nonhomogeneous materials, with a spatially varying material impedance and no thin conducting sheets:

—Material-based limiters, which are coefficients of the extended second-order correction terms, are required for the integration scheme to satisfy the perfect-shift condition in nonhomogeneous materials and, hence, produce the correct wave reflection and transmission at a material interface. These limiters are simply the one-dimensional transmission coefficients for wave propagation in the respective positive and negative grid-coordinate directions. When material-based limiters are not implemented, numerically induced oscillations in the electric and magnetic fields are generated at each cell interface with a discontinuity in the material impedance. The magnitude and frequency of the oscillations are significantly greater at timestep with CFL = 2 than at CFL = 1. The intensity of these oscillations increases as the number of points per wavelength is decreased, and as the discontinuity in the material impedance increases. With material-based limiters, the numerical solution can be obtained at the maximum CFL number prescribed by linear stability analysis, and a smaller number of points per wavelength is required to obtain accurate results.

—At a computational boundary, the extended second-order correction terms exterior to the domain can be defined exactly with respect to the second-order correction terms on the interior. This produces the correct wave propagation across the boundary for waves that exit the computational domain. The result is considerably simplified when material-based limiters are implemented.

In this analysis, with the Maxwell equations written in total-field form, the upwind characteristic-based numerical flux and associated material-based limiters are reformulated to include a thin electric conducting sheet and a thin magnetic conducting sheet at the cell interface. The one-dimensional reflection and transmission coefficients are derived, and the effect of a thin conducting sheet on electromagnetic wave propagation is presented. Numerical results in one dimension are compared to exact analytic solutions to demonstrate the effect that material-based limiters have on numerical wave propagation in nonhomogeneous isotropic materials.

GOVERNING EQUATIONS

Analytic Form

The time-domain Maxwell equations of classical electromagnetics [10] constitute a system of linear hyperbolic partial-differential equations that can be written in the nondimensional vector form

$$\frac{\partial \mathbf{D}}{\partial t} - \nabla \times \mathbf{H} = -\mathbf{J}, \tag{1}$$

$$\frac{\partial \mathbf{B}}{\partial t} + \nabla \times \mathbf{E} = -\mathbf{K}, \tag{2}$$

where the vector $\mathbf{E}$ is the electric field intensity and the vector $\mathbf{H}$ is the magnetic field intensity. $\mathbf{D} = \varepsilon\,\mathbf{E}$ is the electric displacement field vector, and $\mathbf{B} = \mu\mathbf{H}$ is the magnetic induction field vector. The vector $\mathbf{J} = \sigma\,\mathbf{E}$ is the electric field current density, and the vector $\mathbf{K} = \sigma^*\,\mathbf{H}$ is the equivalent magnetic field current density, both of which act to dissipate the energy contained within the electric and magnetic fields. The electric and magnetic properties of the material are defined by the electric permittivity ε and the magnetic permeability μ (which are nondimensionalized by constant free-space values), and the electric conductivity σ and the equivalent magnetic conductivity σ^* (which are nondimensionalized by the free-space material admittance and impedance per unit reference length, respectively).

In this analysis, the material properties are assigned scalar values associated with a linear isotropic material, defined to be independent of the frequency content of the electric and magnetic fields. There are no volumetric EM charge distributions or EM conduction currents, so that $\mathbf{J} = 0$ and $\mathbf{K} = 0$, and the electric and magnetic fields satisfy the divergence conditions $\nabla \cdot \mathbf{D} = 0$ and $\nabla \cdot \mathbf{B} = 0$. However, a thin electric conducting

sheet and a thin magnetic conducting sheet can exist, in which the product of the EM conductivity and sheet thickness is nonzero.

Numerical Form

A CFD-based FV-TD implementation requires that the Maxwell equations (1) and (2) be written as a system of conservation-law statements in Cartesian coordinates. With the chain rule of partial differentiation for the transformation from physical to computational coordinate space, the Maxwell equations can be written in nonorthogonal curvilinear grid-coordinates in the spatially symmetric form

$$\frac{\partial \overline{\mathbf{D}}}{\partial \tau} - \sum_k \frac{\partial \tilde{\mathbf{H}}^k}{\partial k} = 0$$
$$\frac{\partial \overline{\mathbf{B}}}{\partial \tau} + \sum_k \frac{\partial \tilde{\mathbf{E}}^k}{\partial k} = 0 \tag{3}$$

with the geometric conservation law (GCL) constraint

$$\sum_k \frac{\partial \mathbf{N}^k}{\partial k} = 0 \tag{4}$$

where $\tau = t$ is the temporal coordinate, and $k = \xi, \eta, \zeta$ is the generalized curvilinear spatial coordinate, taken in order. $\overline{\mathbf{D}} = V\,\mathbf{D}$ and $\overline{\mathbf{B}} = V\,\mathbf{B}$, in which the metric V is the differential cell volume. The generalized flux vector is defined as

$$\tilde{\mathbf{H}}^k = \mathbf{N}^k \times \mathbf{H}$$
$$\tilde{\mathbf{E}}^k = \mathbf{N}^k \times \mathbf{E} \tag{5}$$

in which the metric $\mathbf{N}^k$ is the differential area vector normal to a k-constant grid-coordinate surface, as the superscript denotes. The electric and magnetic field flux is the vector component of the electric and magnetic fields which is tangent to the grid-coordinate surface. With a finite-volume implementation, V is the cell volume, and $\mathbf{N}^k$ is the cell-face area vector which satisfies the discrete form of the discretization constraint (4), by construction.

MATERIAL COEFFICIENTS

Wave Propogation

With uniform material properties and no EM conduction currents, the symmetry between the electric and magnetic fields allows the Maxwell equations (1) and (2) to be written as an uncoupled system of homogeneous second-order wave equations; hence, a time-varying electromagnetic field propagates with the wave speed

$$c = 1/\sqrt{\varepsilon\,\mu} \tag{6}$$

which is strictly a function of the EM material properties and not the instantaneous EM field strengths. For the propagation of a one-dimensional plane wave in the positive/negative ($\pm$) grid-coordinate direction, the magnetic and electric field vectors are mutually defined as

$$-\mathbf{E} = \pm Z(\hat{\mathbf{N}}^k \times \mathbf{H})$$
$$+\mathbf{H} = \pm Y(\hat{\mathbf{N}}^k \times \mathbf{E}) \tag{7}$$

with $\mathbf{E} \cdot \mathbf{H} = 0$, where $Z = \mu\,c$ is the material impedance, and $Y = \varepsilon\,c$ is the material admittance, which are reciprocal statements, in that $ZY = 1$.

An incident wave can be transmitted (TRNS) and reflected (REFL) at the interface between materials with different electromagnetic properties. The effect of a thin conducting sheet is to instantaneously dissipate energy of the incident wave (independent of the frequency content of the electric and magnetic fields) which is to be distributed to the transmitted and reflected waves. The thin conducting sheet does not induce any phase shift in the transmitted and reflected waves with respect to the incident wave. The reflected and transmitted waves have the same frequency content as the incident wave, so that any change in wave length is in direct proportion to the change in wave speed across the interface.

To describe the physical significance of implementing material-based limiters in a numerical upwind-difference scheme, the one-dimensional transmission and reflection coefficients are derived for grid-aligned wave propagation in the positive/negative ($\pm$) grid-coordinate direction across a material interface designated at $(m \pm 1/2)$. The material interface contains a thin conducting sheet and divides two regions of constant material properties, such that

—For propagation of the incident wave in the (+) grid-coordinate direction, the interface is at $(m + 1/2)$: the material state to the left is designated at (m) and to the right at $(m + 1)$, with all properties of the thin conducting sheet designated at $(m + 1/2)$; the EM field state to the left is designated at $(m + 1/3)$ and to the right at $(m + 2/3)$;

—For propagation of the incident wave in the (−) grid-coordinate direction, the interface is at $(m - 1/2)$: the material state to the right is designated at (m) and to the left at $(m - 1)$, with all properties of the thin conducting sheet designated at $(m - 1/2)$; the EM field state to the right is designated at $(m - 1/3)$ and to the left at $(m - 2/3)$,

where left/right is defined with respect to the positive grid-coordinate direction. By definition, a variable with a non-integer subscript or no subscript denotes a quantity to be evaluated at the $(m + 1/2)$ interface, unless noted otherwise for clarity.

The total field at $(m \pm 1/3)$ and $(m \pm 2/3)$ can be written in terms of the incident wave, and the transmitted and reflected waves. For the magnetic field

$$\begin{aligned}
\tilde{\mathbf{H}}^k_{m\pm 1/3} &= +\,(\tilde{\mathbf{H}}^k_{\mathrm{REFL}} + \tilde{\mathbf{H}}^k_{\mathrm{INC}}) \\
\tilde{\mathbf{H}}^k_{m\pm 2/3} &= +(\tilde{\mathbf{H}}^k_{\mathrm{TRNS}}) \\
\hat{\mathbf{N}}^k \times \tilde{\mathbf{H}}^k_{m\pm 1/3} &= \pm(\tilde{\mathbf{E}}^k_{\mathrm{REFL}} - \tilde{\mathbf{E}}^k_{\mathrm{INC}})\, Y_m \\
\hat{\mathbf{N}}^k \times \tilde{\mathbf{H}}^k_{m\pm 2/3} &= \mp\,(\tilde{\mathbf{E}}^k_{\mathrm{TRNS}})\, Y_{m\pm 1}
\end{aligned} \tag{8}$$

and for the electric field

$$\begin{aligned}
\tilde{\mathbf{E}}^k_{m\pm 1/3} &= +\,(\tilde{\mathbf{E}}^k_{\mathrm{REFL}} + \tilde{\mathbf{E}}^k_{\mathrm{INC}}) \\
\tilde{\mathbf{E}}^k_{m\pm 2/3} &= +(\tilde{\mathbf{E}}^k_{\mathrm{TRNS}}) \\
\hat{\mathbf{N}}^k \times \tilde{\mathbf{E}}^k_{m\pm 1/3} &= \mp(\tilde{\mathbf{H}}^k_{\mathrm{REFL}} - \tilde{\mathbf{H}}^k_{\mathrm{INC}})\, Z_m \\
\hat{\mathbf{N}}^k \times \tilde{\mathbf{E}}^k_{m\pm 2/3} &= \pm(\tilde{\mathbf{H}}^k_{\mathrm{TRNS}})\, Z_{m\pm 1}.
\end{aligned} \tag{9}$$

The tangential component of the magnetic/electric field can be written in terms of the product of the material admittance/impedance and the electric/magnetic field, from Eq. (7), respectively.

Conditions At The Material Interface

With no thin conducting sheet at the material interface, the Maxwell equations require that the tangential vector components of the total electric and magnetic fields be continuous across the interface. The tangential vector components of the total fields are discontinuous across a thin conducting sheet [2, 10]. A thin electric conducting sheet produces a jump in the tangential magnetic field proportional to the electric field current in the sheet. A thin magnetic conducting sheet produces a jump in the tangential electric field proportional to the magnetic field current in the sheet. The conditions across the material interface at $(m \pm 1/2)$ can be written in the general form

$$\begin{aligned}
[\![\tilde{\mathbf{H}}^k]\!]_{m\pm 1/2} &= -(\sigma\, d)\hat{\mathbf{N}}^k \times \tilde{\mathbf{E}}^{\mathrm{AVG}}_{m\pm 1/2} \\
[\![\tilde{\mathbf{E}}^k]\!]_{m\pm 1/2} &= +(\sigma^* d)\, \hat{\mathbf{N}}^k \times \tilde{\mathbf{H}}^{\mathrm{AVG}}_{m\pm 1/2}
\end{aligned} \tag{10}$$

which is equivalent to

$$\begin{aligned}
\hat{\mathbf{N}}^k \times [\![\tilde{\mathbf{H}}^k]\!]_{m\pm 1/2} &= +(\sigma\, d)\, \tilde{\mathbf{E}}^{\mathrm{AVG}}_{m\pm 1/2} \\
\hat{\mathbf{N}}^k \times [\![\tilde{\mathbf{E}}^k]\!]_{m\pm 1/2} &= -(\sigma^* d)\, \tilde{\mathbf{H}}^{\mathrm{AVG}}_{m\pm 1/2}.
\end{aligned} \tag{11}$$

The jump conditions are defined with respect to the positive grid-coordinate direction as

$$\begin{aligned}
[\![\tilde{\mathbf{H}}^k]\!]_{m\pm 1/2} &= \pm(\tilde{\mathbf{H}}^k_{m\pm 2/3} - \tilde{\mathbf{H}}^k_{m\pm 1/3}) \\
[\![\tilde{\mathbf{E}}^k]\!]_{m\pm 1/2} &= \pm(\tilde{\mathbf{E}}^k_{m\pm 2/3} - \tilde{\mathbf{E}}^k_{m\pm 1/3}).
\end{aligned} \tag{12}$$

The quantity $(\sigma\, d)$ is the electric conductivity and the quantity $(\sigma^* d)$ is the equivalent magnetic conductivity, with $(\sigma\, d) \geq 0$ and $(\sigma^* d) \geq 0$ by definition, where d is the thickness of each sheet. The electric field in the thin electric conducting sheet and the magnetic field in the thin magnetic conducting sheet can be written as a weighted average of the respective values at $(m \pm 1/3)$ and $(m \pm 2/3)$; consequently,

$$\begin{aligned}
\tilde{\mathbf{E}}^{\mathrm{AVG}}_{m\pm 1/2} &= \tilde{\mathbf{E}}^k_{m\pm 1/3} \pm \mathcal{A}_2^{\pm}\, [\![\tilde{\mathbf{E}}^k]\!]_{m\pm 1/2} \\
&= \mathcal{A}_1^{\pm}\, \tilde{\mathbf{E}}^k_{m\pm 1/3} + \mathcal{A}_2^{\pm}\, \tilde{\mathbf{E}}^k_{m\pm 2/3} \\
\tilde{\mathbf{H}}^{\mathrm{AVG}}_{m\pm 1/2} &= \tilde{\mathbf{H}}^k_{m\pm 1/3} \pm \mathcal{A}_1^{\pm}\, [\![\tilde{\mathbf{H}}^k]\!]_{m\pm 1/2} \\
&= \mathcal{A}_2^{\pm}\, \tilde{\mathbf{H}}^k_{m\pm 1/3} + \mathcal{A}_1^{\pm}\, \tilde{\mathbf{H}}^k_{m\pm 2/3},
\end{aligned} \tag{13}$$

where $\mathcal{A}_1^{\pm} + \mathcal{A}_2^{\pm} = 1$, with $\mathcal{A}_1^{\pm} \geq 0$ and $\mathcal{A}_2^{\pm} \geq 0$, in that

$$\begin{aligned}
\mathcal{A}_1^{+} &= \mathcal{A}_1, \quad \mathcal{A}_2^{+} = \mathcal{A}_2 \quad \text{at } (m + \tfrac{1}{2}) \\
\mathcal{A}_1^{-} &= \mathcal{A}_2, \quad \mathcal{A}_2^{-} = \mathcal{A}_1 \quad \text{at } (m - \tfrac{1}{2})
\end{aligned}$$

The coefficients $\mathcal{A}_1$ and $\mathcal{A}_2$ are weight factors defined with respect to the positive grid-coordinate direction, which introduces an additional directional dependence with respect to the wave propagation direction. In this analysis, the coefficients $\mathcal{A}_1$ and $\mathcal{A}_2$ are simple scalar constants, but there is no restriction in defining these terms to be a more complex function of some material property. To substantiate the formulation of Eq. (13):

—When $(\sigma\, d) \neq 0$ and $(\sigma^* d) = 0$, the tangential component of the total electric field is continuous and the tangential component of the total magnetic field is discontinuous across the electric conducting sheet; hence, the electric field in the conducting sheet is evaluated at $(m \pm 1/3)$ or equivalently at $(m \pm 2/3)$, and results are independent of $\mathcal{A}_1$ and $\mathcal{A}_2$.

—When $(\sigma\, d) = 0$ and $(\sigma^* d) \neq 0$, the tangential component of the total magnetic field is continuous and the tangential component of the total electric field is discontinuous across the magnetic conducting sheet; hence, the magnetic field in the conducting sheet is evaluated at $(m \pm 1/3)$ or equivalently at $(m \pm 2/3)$, and results are independent of $\mathcal{A}_1$ and $\mathcal{A}_2$.

—When $(\sigma\, d) \neq 0$ and $(\sigma^* d) \neq 0$, then the tangential components of the electric and magnetic fields are discontinuous, and results are strongly dependent on the weight factors $\mathcal{A}_1$ and $\mathcal{A}_2$. If the electric conducting sheet is left/right of the interface at $(m \pm 1/3)$ and the magnetic conducting sheet is right/left of the interface at $(m \pm 2/3)$, then

$$\begin{aligned}
\tilde{\mathbf{E}}^{\mathrm{AVG}}_{m\pm 1/2} &= \tilde{\mathbf{E}}^k_{m\pm 1/3} \\
\tilde{\mathbf{H}}^{\mathrm{AVG}}_{m\pm 1/2} &= \tilde{\mathbf{H}}^k_{m\pm 2/3}
\end{aligned}$$

which is obtained for $\mathcal{A}_1^{\pm} = 1$ and $\mathcal{A}_2^{\pm} = 0$. If the magnetic conducting sheet is left/right of the interface at $(m \pm 1/3)$ and

the electric conducting sheet is right/left of the interface at ($m \pm 2/3$), then

$$\tilde{\mathbf{E}}^{\mathrm{AVG}}_{m\pm 1/2} = \tilde{\mathbf{E}}^{k}_{m\pm 2/3}$$

$$\tilde{\mathbf{H}}^{\mathrm{AVG}}_{m\pm 1/2} = \tilde{\mathbf{H}}^{k}_{m\pm 1/3}$$

which is obtained for $\mathcal{A}_1^{\pm} = 0$ and $\mathcal{A}_2^{\pm} = 1$. An intermediate state between these extremes is obtained for $\mathcal{A}_1^{\pm}$ and $\mathcal{A}_2^{\pm}$ not equal to zero or one.

TRNS/REFL and LOSS Coefficients

The reflection/transmission coefficient is the ratio of the amplitude of the reflected/transmitted wave to the amplitude of the incident wave. These coefficients are derived by substituting the total magnetic and electric fields (8) and (9) at ($m \pm 1/3$) and ($m \pm 2/3$) into the interface conditions (10) and (11). With these operations, the reflection and transmission coefficients become

$$(Z^{\pm}_{\mathrm{REFL}})_{m\pm 1/2} = \frac{A_{11}Z_m - B_{11}Z_{m\pm 1}}{A_{11}Z_m + B_{11}Z_{m\pm 1}}$$

$$(Z^{\pm}_{\mathrm{TRNS}})_{m\pm 1/2} = \frac{2A_{12}Z_m}{A_{11}Z_m + B_{11}Z_{m\pm 1}} \tag{14}$$

for the magnetic field and

$$(Y^{\pm}_{\mathrm{REFL}})_{m\pm 1/2} = \frac{B_{11}Y_m - A_{11}Y_{m\pm 1}}{B_{11}Y_m + A_{11}Y_{m\pm 1}}$$

$$(Y^{\pm}_{\mathrm{TRNS}})_{m\pm 1/2} = \frac{2B_{12}Y_m}{B_{11}Y_m + A_{11}Y_{m\pm 1}} \tag{15}$$

for the electric field. The coefficients A and B are defined respectively by Eq. (23) and Eq. (25), when the numerical flux is derived. These terms are equal to one with zero conductivity, so that the reflection and transmission coefficients for a material interface with no conducting sheet are recovered.

The total energy within the incident wave is not conserved across a thin conducting sheet. A measure of the energy in the respective magnetic and electric fields that is absorbed by the conducting sheet can be written as

$$Z^{\pm}_{\mathrm{TRNS}} - Z^{\pm}_{\mathrm{REFL}} = 1 - Z^{\pm}_{\mathrm{LOSS}}$$

$$Y^{\pm}_{\mathrm{TRNS}} - Y^{\pm}_{\mathrm{REFL}} = 1 - Y^{\pm}_{\mathrm{LOSS}} \tag{16}$$

where the loss (LOSS) coefficients are defined as

$$(Z^{\pm}_{\mathrm{LOSS}})_{m\pm 1/2} = \frac{2(A_{11} - A_{12})Z_m}{A_{11}Z_m + B_{11}Z_{m\pm 1}}$$

$$(Y^{\pm}_{\mathrm{LOSS}})_{m\pm 1/2} = \frac{2(B_{11} - B_{12})Y_m}{B_{11}Y_m + A_{11}Y_{m\pm 1}} \tag{17}$$

such that $Z_{\mathrm{LOSS}} \geq 0$ and $Y_{\mathrm{LOSS}} \geq 0$. With no thin conducting sheet, then $Z_{\mathrm{LOSS}} = 0$ and $Y_{\mathrm{LOSS}} = 0$ which means the total energy of the incident wave is conserved.

Properties of the Conducting Sheet

The material properties that are required to produce no reflection of the incident wave can be derived by setting the numerator of the reflection coefficients (14) and (15) equal to zero, which produces a quadratic equation to be solved for $\mathcal{A}_1^{\pm}$ or $\mathcal{A}_2^{\pm}$. For homogeneous constant material properties, this expression can be written as

$$(\mathcal{A}_2^{\pm} - \mathcal{A}_1^{\pm})(\sigma d)(\sigma^* d) = Z(\sigma d) - Y(\sigma^* d).$$

An equivalent result is produced when the energy loss is defined to be equally distributed between the electric and magnetic fields. For equal electric and magnetic conductivity and free-space conditions $Z = Y$, then $\mathcal{A}_1^{\pm} = 1/2$.

To derive the material properties required to produce no transmission of the incident wave, the numerator of the transmission coefficients (14) and (15) are set equal to zero; hence, with nonzero conductivity

$$\mathcal{A}_1^{\pm}\,\mathcal{A}_2^{\pm}(\sigma d)(\sigma^* d) = 1$$

Consequently, the incident wave is totally absorbed by the conducting sheet when $(\sigma d) = 2$ and $(\sigma^* d) = 2$.

NUMERICAL FLUX

The numerical flux prescribed by Shankar *et al.* [1–5] is defined by a characteristic-based integration that represents the exact solution of a one-dimensional Riemann problem, in which the respective left and right states at the cell interface are cell-averaged quantities: the electric and magnetic vector fields and material properties.

At interface ($m \pm 1/2$), a path of integration is constructed in the space–time plane to connect the left/right state at cell (m) to the right/left state at cell ($m \pm 1$) at time level (n). The path is divided into contiguous sub-paths that connect the left and right states to the sub-states at ($m \pm 1/3$) and ($m \pm 2/3$) at time level ($n + 1/2$). The sub-path from (m) to ($m \pm \frac{1}{3}$) is along the ($\pm$) wave-type characteristic across the ($\mp$) wave-fields. The sub-path from ($m \pm 2/3$) to ($m \pm 1$) is along the ($\mp$) wave-type characteristic across the ($\pm$) wave-fields. The sub-path along the stream-type characteristic connects the sub-states at ($m \pm 1/3$) and ($m \pm 2/3$). For a linear system of equations, the wave speed is constant along each sub-path; hence, the numerical flux is the sub-state which divides the negative and positive wave-fields. The sub-state at ($m \pm 1/3$) is the flux at the ($m \pm 1/2$) interface for cell (m), and the sub-state at ($m \pm 2/3$) is the flux at the ($m \pm 1/2$) interface for

cell ($m \pm 1$). The flux is continuous across the interface when the sub-states at ($m \pm 1/3$) and ($m \pm 2/3$) are equivalent [7, 8].

From a one-dimensional characteristic-based analysis of the Maxwell equations, the cell-averaged material properties and Riemann invariants are constant along the ($\pm$) wave-type characteristics (eigenvalue). For the electric and magnetic fields, integration of the compatibility equations from (m) to ($m \pm 1/3$) can be written as

$$\begin{aligned}(r\tilde{\mathbf{H}}^{\pm})_{m\pm1/3} - (r\tilde{\mathbf{H}}^{\pm})_m &= 0\\ (r\tilde{\mathbf{E}}^{\pm})_{m\pm1/3} - (r\tilde{\mathbf{E}}^{\pm})_m &= 0\end{aligned} \tag{18}$$

with the Riemann invariants of the ($\pm$) wave-type characteristic defined in vector form as

$$\begin{aligned}(r\tilde{\mathbf{H}}^{\pm})_m &= +Z_m\tilde{\mathbf{H}}^k_m \pm \hat{\mathbf{N}}^k \times \tilde{\mathbf{E}}^k_m\\ (r\tilde{\mathbf{E}}^{\pm})_m &= -Y_m\tilde{\mathbf{E}}^k_m \pm \hat{\mathbf{N}}^k \times \tilde{\mathbf{H}}^k_m.\end{aligned} \tag{19}$$

An important property of the Riemann invariants is the ability to recognize the direction of wave propagation, such that $(r\tilde{\mathbf{H}}^{\pm}) = 0$ and $(r\tilde{\mathbf{E}}^{\pm}) = 0$ for the propagation of a one-dimensional plane wave in the negative/positive ($\mp$) grid-coordinate direction. To define the electric and magnetic field sub-states, from Eq. (18):

Along the ($\pm$) wave-type characteristic from cell (m) to the sub-state at ($m \pm 1/3$), then

$$\begin{aligned}(r\tilde{\mathbf{H}}^{\pm})_m &= (r\tilde{\mathbf{H}}^{\pm})_{m\pm1/3}\\ &= +Z_m\tilde{\mathbf{H}}^k_{m\pm1/3} \pm \hat{\mathbf{N}}^k \times \tilde{\mathbf{E}}^k_{m\pm1/3}\\ (r\tilde{\mathbf{E}}^{\pm})_m &= (r\tilde{\mathbf{E}}^{\pm})_{m\pm1/3}\\ &= -Y_m\tilde{\mathbf{E}}^k_{m\pm1/3} \pm \hat{\mathbf{N}}^k \times \tilde{\mathbf{H}}^k_{m\pm1/3}.\end{aligned} \tag{20}$$

Along the ($\mp$) wave-type characteristic from cell ($m \pm 1$) to the sub-state at ($m \pm 2/3$), then

$$\begin{aligned}(r\tilde{\mathbf{H}}^{\mp})_{m\pm1} &= (r\tilde{\mathbf{H}}^{\mp})_{m\pm2/3}\\ &= +Z_{m\pm1}\tilde{\mathbf{H}}^k_{m\pm2/3} \mp \hat{\mathbf{N}}^k \times \tilde{\mathbf{E}}^k_{m\pm2/3}\\ (r\tilde{\mathbf{E}}^{\mp})_{m\pm1} &= (r\tilde{\mathbf{E}}^{\mp})_{m\pm2/3}\\ &= -Y_{m\pm1}\tilde{\mathbf{E}}^k_{m\pm2/3} \mp \hat{\mathbf{N}}^k \times \tilde{\mathbf{H}}^k_{m\pm2/3}.\end{aligned} \tag{21}$$

The numerical flux is the simultaneous solution of the characteristic equations (20) and (21) and interface conditions (10) and (11). With no thin conducting sheet, the flux is continuous between the sub-states at ($m \pm 1/3$) and ($m \pm 2/3$). With a thin electric/magnetic conducting sheet, the magnetic/electric field flux is discontinuous between ($m \pm 1/3$) and ($m \pm 2/3$).

Solving for $\tilde{\mathbf{H}}^k$ and $\hat{\mathbf{N}}^k \times \tilde{\mathbf{E}}^k$, the numerical flux for the magnetic field can be written as

$$\begin{aligned}\tilde{\mathbf{H}}^k_{m\pm1/3} &= +\frac{A_{11}(r\tilde{\mathbf{H}}^{\pm})_m + A_{12}(r\tilde{\mathbf{H}}^{\mp})_{m\pm1}}{A_{11}Z_m + B_{11}Z_{m\pm1}}\\ \tilde{\mathbf{H}}^k_{m\pm2/3} &= +\frac{A_{21}(r\tilde{\mathbf{H}}^{\pm})_m + A_{22}(r\tilde{\mathbf{H}}^{\mp})_{m\pm1}}{B_{22}Z_m + A_{22}Z_{m\pm1}},\end{aligned} \tag{22}$$

where $A_{11}Z_m + B_{11}Z_{m\pm1} = B_{22}Z_m + A_{22}Z_{m\pm1}$, and

$$\begin{aligned}A_{11} &= A_{12} + (\sigma d)\,[\mathcal{A}_1^{\pm}(\sigma^* d) + Z_{m\pm1}]\\ A_{12} &= 1 - \mathcal{A}_1^{\mp}\mathcal{A}_2^{\pm}(\sigma d)(\sigma^* d)\\ A_{21} &= 1 - \mathcal{A}_2^{\pm}\mathcal{A}_1^{\pm}(\sigma d)(\sigma^* d)\\ A_{22} &= A_{21} + (\sigma d)\,[\mathcal{A}_2^{\pm}(\sigma^* d) + Z_m].\end{aligned} \tag{23}$$

Solving for $\tilde{\mathbf{E}}^k$ and $\hat{\mathbf{N}}^k \times \tilde{\mathbf{H}}^k$, the numerical flux for the electric field can be written as

$$\begin{aligned}\tilde{\mathbf{E}}^k_{m\pm1/3} &= -\frac{B_{11}(r\tilde{\mathbf{E}}^{\pm})_m + B_{12}(r\tilde{\mathbf{E}}^{\mp})_{m\pm1}}{B_{11}Y_m + A_{11}Y_{m\pm1}}\\ \tilde{\mathbf{E}}^k_{m\pm2/3} &= -\frac{B_{21}(r\tilde{\mathbf{E}}^{\pm})_m + B_{22}(r\tilde{\mathbf{E}}^{\mp})_{m\pm1}}{A_{22}Y_m + B_{22}Y_{m\pm1}},\end{aligned} \tag{24}$$

where $B_{11}Y_m + A_{11}Y_{m\pm1} = A_{22}Y_m + B_{22}Y_{m\pm1}$, and

$$\begin{aligned}B_{11} &= B_{12} + (\sigma^* d)[\mathcal{A}_2^{\pm}(\sigma d) + Y_{m\pm1}]\\ B_{12} &= 1 - \mathcal{A}_1^{\pm}\mathcal{A}_2^{\pm}(\sigma^* d)(\sigma d)\\ B_{21} &= 1 - \mathcal{A}_2^{\mp}\mathcal{A}_1^{\pm}(\sigma^* d)(\sigma d)\\ B_{22} &= B_{21} + (\sigma^* d)\,[\mathcal{A}_1^{\pm}(\sigma d) + Y_m].\end{aligned} \tag{25}$$

The numerical flux (22) and (24) is a nonlocal quantity that represents the exchange of cell-averaged information between (m) and ($m \pm 1$) across the material interface. The material coefficients (23) and (25) are a function of the sheet conductivity at ($m \pm 1/2$) and the material impedance and admittance at (m) and ($m \pm 1$). When the sheet conductivity is zero, the numerical flux for an interface with no thin conducting sheet is recovered.

INTEGRATION ALGORITHM

The explicit predictor–corrector scheme developed by Warming and Beam [6] is used to integrate the Maxwell equations [1–5], with the material-based limiters derived by Bishop and Anderson [9] included as coefficients on the extended second-order correction terms in the corrector step. New mate-

rial-based limiters are presented to account for the thin electric and thin magnetic conducting sheets in the numerical flux.

Predictor:

$$(\overline{\mathbf{D}})_m^{\overline{n+1}} = (\overline{\mathbf{D}})_m^n + \frac{\Delta\tau}{\Delta k}(\Delta\tilde{\mathbf{H}})_m^n$$
$$(\overline{\mathbf{B}})_m^{\overline{n+1}} = (\overline{\mathbf{B}})_m^n - \frac{\Delta\tau}{\Delta k}(\Delta\tilde{\mathbf{E}})_m^n. \tag{26}$$

Corrector:

$$\begin{aligned}(\overline{\mathbf{D}})_m^{n+1} = (\overline{\mathbf{D}})_m^n &+ \frac{1}{2}\frac{\Delta\tau}{\Delta k}[(\Delta\tilde{\mathbf{H}})_m^{\overline{n+1}} + (\Delta\tilde{\mathbf{H}})_m^n] \\ &+ \frac{1}{2}\frac{\Delta\tau}{\Delta k}\sum_k [(X_z^+\, d\tilde{\mathbf{H}}^+)_{m-1/2}^n] \\ &+ \frac{1}{2}\frac{\Delta\tau}{\Delta k}\sum_k [(Z^+\, d\tilde{\mathbf{H}}^+)_{m-1/2}^n - (Z^+\, d\tilde{\mathbf{H}}^+)_{m-3/2}^n] \\ &+ \frac{1}{2}\frac{\Delta\tau}{\Delta k}\sum_k [(Z^-\, d\tilde{\mathbf{H}}^-)_{m+1/2}^n - (Z^-\, d\tilde{\mathbf{H}}^-)_{m+3/2}^n] \\ &+ \frac{1}{2}\frac{\Delta\tau}{\Delta k}\sum_k [(X_z^-\, d\tilde{\mathbf{H}}^-)_{m+1/2}^n];\end{aligned}$$
$$\begin{aligned}(\overline{\mathbf{B}})_m^{n+1} = (\overline{\mathbf{B}})_m^n &- \frac{1}{2}\frac{\Delta\tau}{\Delta k}[(\Delta\tilde{\mathbf{E}})_m^{\overline{n+1}} + (\Delta\tilde{\mathbf{E}})_m^n] \\ &- \frac{1}{2}\frac{\Delta\tau}{\Delta k}\sum_k [(X_Y^+\, d\tilde{\mathbf{E}}^+)_{m-1/2}^n] \\ &- \frac{1}{2}\frac{\Delta\tau}{\Delta k}\sum_k [(Y^+\, d\tilde{\mathbf{E}}^+)_{m-1/2}^n - (Y^+\, d\tilde{\mathbf{E}}^+)_{m-3/2}^n] \\ &- \frac{1}{2}\frac{\Delta\tau}{\Delta k}\sum_k [(Y^-\, d\tilde{\mathbf{E}}^-)_{m+1/2}^n - (Y^-\, d\tilde{\mathbf{E}}^-)_{m+3/2}^n] \\ &- \frac{1}{2}\frac{\Delta\tau}{\Delta k}\sum_k [(X_Y^-\, d\tilde{\mathbf{E}}^-)_{m+1/2}^n],\end{aligned} \tag{27}$$

in which $\Delta k = 1$ and $\Delta\tau$ = timestep, by definition. The subscript (m) is the index associated with the spatial curvilinear grid-coordinate, and the superscript (n) is the index associated with the temporal coordinate. An integer subscript denotes cell-centroid information, and a noninteger subscript denotes cell-interface information. The extended second-order correction terms for the magnetic and electric field flux are defined as

$$(d\tilde{\mathbf{H}}^{\mp})_{m\pm1/2} = \mp(\mathbf{N}_{m\pm1/2}^k \times \mathbf{H}_m - \tilde{\mathbf{H}}_{m\pm1/3}^k)$$
$$(d\tilde{\mathbf{E}}^{\mp})_{m\pm1/2} = \mp(\mathbf{N}_{m\pm1/2}^k \times \mathbf{E}_m - \tilde{\mathbf{E}}_{m\pm1/3}^k). \tag{28}$$

The terms $Z^{\pm}$ and $Y^{\pm}$ and $X^{\pm}$ are the material-based limiters. To state that these limiters are not implemented is equivalent to setting $Z^{\pm} = Y^{\pm} = 1$ and $X^{\pm} = 0$ for all variations of material properties, which recovers the original integration scheme.

For cell (m) with interface at $(m + 1/2)$ and $(m - 1/2)$, evaluating the spatial derivatives for each computational coordinate is equivalent to integrating the numerical flux over the bounding surface. The flux residual can be written in standard form as

$$(\Delta\tilde{\mathbf{H}})_m = \sum_k [\tilde{\mathbf{H}}_{m+1/3}^k - \tilde{\mathbf{H}}_{m-1/3}^k]$$
$$(\Delta\tilde{\mathbf{E}})_m = \sum_k [\tilde{\mathbf{E}}_{m+1/3}^k - \tilde{\mathbf{E}}_{m-1/3}^k], \tag{29}$$

or, equivalently, as

$$(\Delta\tilde{\mathbf{H}})_m = \sum_k [(d\tilde{\mathbf{H}}^-)_{m+1/2}^n + (d\tilde{\mathbf{H}}^+)_{m-1/2}^n]$$
$$(\Delta\tilde{\mathbf{E}})_m = \sum_k [(d\tilde{\mathbf{E}}^-)_{m+1/2}^n + (d\tilde{\mathbf{E}}^+)_{m-1/2}^n], \tag{30}$$

so that the predictor–corrector sequence can be written strictly in terms of the second-order corrections (28). The standard subscript $(m \pm 1/2)$ has been replaced with subscript $(m \pm 1/3)$ to indicate that the numerical flux (22) and (24) may be discontinuous at the cell interface.

The predictor step alone is a first-order accurate explicit scheme, which is stable for CFL ≤ 1. The predictor–corrector sequence, together with the extended second-order correction terms, makes the scheme second-order accurate in space and time. The predictor–corrector scheme is stable for CFL ≤ 2. The CFL number at cell-m is defined in multiple dimensions as

$$\mathrm{CFL} = \left(c\frac{\Delta\tau}{\Delta k}\right)\frac{1}{V_m}\sum_k \frac{1}{2}(A_{m+1/2} + A_{m-1/2}), \tag{31}$$

where $A_{m\pm1/2}$ is the area magnitude of the cell face at $(m \pm 1/2)$.

MATERIAL-BASED LIMITERS

For one-dimensional wave propagation, the numerical and exact analytic solutions will be equivalent when the integration scheme satisfies the perfect-shift condition (no numerically induced dissipation or dispersion). For all variations of the material properties, the predictor scheme satisfies the perfect-shift condition at CFL = 1, and the predictor–corrector scheme satisfies perfect-shift condition at CFL = 1 and CFL = 2 provided the material-based limiters are implemented.

The material-based limiters are derived by forcing the predictor-corrector scheme to satisfy the perfect-shift condition at CFL = 1 and CFL = 2 for all variations of the material properties at $(m \pm 1/2)$ and $(m \pm 3/2)$ between consecutive cells. The required algebraic manipulations are considerably

simplified by substituting into the numerical flux of corrector step the identities

$$(r\tilde{\mathbf{H}}^{\pm})_m^{\overline{n+1}} = (r\tilde{\mathbf{H}}^{\pm})_m^n \mp \alpha\, Z_m (d\tilde{\mathbf{H}}^{\pm})_{m\mp 1/2}^n$$
$$(r\tilde{\mathbf{E}}^{\pm})_m^{\overline{n+1}} = (r\tilde{\mathbf{E}}^{\pm})_m^n + \alpha\, Y_m (d\tilde{\mathbf{E}}^{\pm})_{m\mp 1/2}^n, \tag{32}$$

where $\alpha = 2$ (CFL). For one-dimensional wave propagation the predictor step alone is exactly equivalent to the predictor–corrector sequence at CFL = 1; and similarly, implementing the predictor step alone for two time steps at CFL = 1 is exactly equivalent to implementing the predictor–corrector sequence for one time step at CFL = 2 [9].

With a thin electric conducting sheet and-or a thin magnetic conducting sheet at the material interface ($m \pm 1/2$), the material-based limiters can be written as

$$\begin{aligned}
(Z^{\pm})_{m\mp 1/2} &= \frac{2A_{12}Z_m}{A_{11}Z_m + B_{11}Z_{m\pm 1}} \\
&= (Z^{\pm}_{\mathrm{TRNS}})_{m\pm 1/2} \\
(Y^{\pm})_{m\mp 1/2} &= \frac{2B_{12}Y_m}{B_{11}Y_m + A_{11}Y_{m\pm 1}}; \\
&= (Y^{\pm}_{\mathrm{TRNS}})_{m\pm 1/2} \qquad (33) \\
(X^{\pm}_{\tilde{Z}})_{m\mp 1/2} &= \frac{2(A_{11} - A_{12})Z_m}{A_{11}Z_m + B_{11}Z_{m\pm 1}} \\
&= (Z^{\pm}_{\mathrm{LOSS}})_{m\pm 1/2} \\
(X^{\pm}_{\tilde{Y}})_{m\mp 1/2} &= \frac{2(B_{11} - B_{12})Y_m}{B_{11}Y_m + A_{11}Y_{m\pm 1}} \\
&= (Y^{\pm}_{\mathrm{LOSS}})_{m\pm 1/2} \qquad (34)
\end{aligned}$$

which are functions of the material properties and not the instantaneous electric or magnetic field strengths. The material-based limiters at ($m \mp 1/2$) are the transmission coefficients (14) and (15) and loss coefficients (17) for wave propagation in the positive/negative ($\pm$) grid-coordinate direction across the material interface at ($m \pm 1/2$). Similarly, the material-based limiters at ($m \mp 3/2$) are the transmission coefficients for wave propagation in the positive/negative ($\pm$) grid-coordinate direction across the material interface at ($m \mp 1/2$); in other words, only information at ($m \mp 3/2$) that is transmitted across the ($m \mp 1/2$) interface can be used in the integration of the electric and magnetic fields at cell (m). Because of this physical significance, the implementation is valid for noninteger CFL numbers and wave propagation in multiple dimensions.

The implementation of material-based limiters enables the predictor–corrector sequence to properly account for the multiple reflections and energy loss that occur in the integration of the electric and magnetic fields from time level (n) to ($n + 1$). From a more general perspective, the spatial extrapolation across consecutive cells that is used to obtain better than first-order spatial accuracy must account for the wave reflection and transmission due to the change in material impedance across the cell interface. For the predictor–corrector integration scheme, in addition to the characteristic-based numerical flux, this was done explicitly by the addition of scalar coefficients, called material-based limiters, on the second-order correction terms.

BOUNDARY CONDITIONS

The computational domain is of finite extent so that boundary conditions must be specified at the domain boundaries. For cell (m) on a max-k boundary, the numerical flux at ($m + 1/2$) and the second-order corrections at ($m + 3/2$) are required; for cell (m) on a min-k boundary, the numerical flux at ($m - 1/2$) and the second-order corrections at ($m - 3/2$) are required. The subscript BC is used to denote the boundary at (m $\pm$ 1/2) for cell (m).

For an electromagnetic wave that originates from the domain interior to pass through the computational boundary without undue reflection, the Riemann invariant associated with all incoming waves is set equal to zero; hence,

$$(r\tilde{\mathbf{H}}^{\mp})_{m\pm 1} = 0$$
$$(r\tilde{\mathbf{E}}^{\mp})_{m\pm 1} = 0 \tag{35}$$

which is exact for one-dimensional wave motion normal to the boundary. This condition can be substituted into the numerical flux (22) and (24) for the electric and magnetic fields; hence,

$$\tilde{\mathbf{H}}^k_{\mathrm{BC}} = +\frac{A_{11}(r\tilde{\mathbf{H}}^{\pm})_m}{A_{11}Z_m + B_{11}Z_{m\pm 1}}$$
$$\tilde{\mathbf{E}}^k_{\mathrm{BC}} = -\frac{B_{11}(r\tilde{\mathbf{E}}^{\pm})_m}{B_{11}Y_m + A_{11}Y_{m\pm 1}}. \tag{36}$$

The material properties designated at ($m \pm 1$) represent an impedance boundary condition with respect to the material properties at (m) and the properties of the thin conducting sheet on the boundary. With the appropriate specification of material properties at (m) and ($m \pm 1$) and properties of the conducting sheet at ($m \pm 1/2$), the boundary condition flux (36) can be applied to a computational boundary which is farfield or at the surface of a perfect electric-conducting body.

Given the numerical flux (36) at the computational boundary, the second-order corrections (28) at ($m \pm 3/2$) can be defined with the same approach used to derive the material-based limiters (33). With the implementation of material-based limiters, this produces

$$(d\tilde{\mathbf{H}}^{\mp})_{m\pm 3/2} = 0$$
$$(d\tilde{\mathbf{E}}^{\mp})_{m\pm 3/2} = 0; \tag{37}$$

otherwise,

$$(d\tilde{\mathbf{H}}^{\mp})_{m\pm 3/2} = -(Z^{\pm}_{\mathrm{REFL}})_{m\pm 1/2}\,(d\tilde{\mathbf{H}}^{\pm})_{m\mp 1/2}$$
$$(d\tilde{\mathbf{E}}^{\mp})_{m\pm 3/2} = -(Y^{\pm}_{\mathrm{REFL}})_{m\pm 1/2}(d\tilde{\mathbf{E}}^{\pm})_{m\mp 1/2}. \tag{38}$$

The $(\mp)$ extended second-order correction terms exterior to the domain are defined exactly in terms of the $(\pm)$ correction terms on the domain interior, with the reflection coefficients (14) and (15) for propagation of the magnetic and electric fields in the $(\pm)$ grid-coordinate direction [9].

NUMERICAL RESULTS

To clearly demonstrate the effect of implementing material-based limiters, wave propagation in one dimension across a single material interface is studied. The grid spacing satisfies the constraint that the cell volume divided by the wave speed is equal to one (constant). The computational domain is divided into two regions of constant material properties, with an interface at $x = 0$ that may contain a thin conducting sheet: region-I for $x < 0$ is free-space, and region-II for $x > 0$ is to be defined. The incident wave is a second-derivative continuous pulse defined at time zero as

$$\mathbf{E} = \sum_{n=0}^{n=3} \alpha_n \cos(2\pi n\bar{x}) \tag{39}$$

for $0.0 \leq \bar{x} \leq 1.0$, such that

$$\alpha_0 = +0.43750$$
$$\alpha_1 = -0.53125$$
$$\alpha_2 = +0.06250$$
$$\alpha_3 = +0.03125.$$

The pulse is contained within 26 cells, with the highest frequency contained within approximately 8 cells. At time zero, the center of the pulse is located approximately 10.5 pulse widths left of the interface. This enables a reasonably fair comparison of the distortions introduced by the predictor–corrector scheme as the result of the inherent dispersion and dissipation at noninteger CFL numbers for the specified number of integration steps, and not implementing material-based limiters in regions with a spatially varying material impedance. Because it is important to advance the solution at the maximum timestep to minimize CPU requirements, only CFL numbers in the range $1.0 \leq \mathrm{CFL} \leq 2.0$ are implemented.

Numerical results are presented for the following three fundamental material interface configurations: (1) a material interface with no conducting sheet, shown in Fig. 2 and Fig. 3; (2) a thin electric and magnetic conducting sheet with no material interface, shown Fig. 4; and (3) a material interface with a thin electric and magnetic conducting sheet, shown in Fig. 5. Each figure contains solutions for two CFL numbers and two sets of material properties to demonstrate the effect of the timestep and magnitude of the impedance discontinuity on the solution error. Each plot contains the incident pulse traveling in the positive coordinate direction, and the transmitted and reflected pulses generated by the change in material impedance (an arrow indicates the direction of propagation). The incident pulse and reflected pulse are shown at the same spatial position, approximately one pulse width from the interface, after traveling 9.5 and 11.5 pulse widths, respectively. Only the electric field is shown at different time levels, since the magnetic field is the electric field divided by the material impedance. A solid line denotes the solution when material-based limiters are implemented (which is equivalent to the exact solution at integer CFL numbers), and a dashed line denotes the solution computed without material-based limiters. The plotted error in the reflected and transmitted waves is the difference between the numerical solutions with and without material-based limiters.

Figure 2 presents solutions (a) at CFL = 1.0, 2.0 with $\varepsilon = 36$ and $\mu = 1$, and (b) at CFL = 1.5, 2.0 with $\varepsilon = 49$ and $\mu = 1$. The error at CFL = 1.0 and CFL = 1.5 is negligible for this set of material properties, even when compared to the distortion at CFL = 1.5 due to the numerical dispersion. At CFL = 2.0, the reflected and transmitted waves are distorted by the oscillations generated at the cell interface when material-based limiters are not implemented. The relative magnitude of these oscillations is greater than the distortion introduced by the dispersion at noninteger CFL numbers, and increases dramatically as the impedance is increased. A greater material impedance will produce oscillations that completely overpower the reflected and transmitted pulses so that they cannot be distinguished. Solutions for a larger discontinuity in the material impedance can only be obtained when CFL $\leq$ 2.0. Figure 3 presents solutions (a) at CFL = 1.5, 1.9 with $\varepsilon = 81$ and $\mu = 1$, and (b) at CFL = 1.5, 1.8 with $\varepsilon = 196$ and $\mu = 1$, which exhibit the same behavior described previously. These results indicated that the implementation of material-based limiters is required only for geometries with relatively large discontinuities in the material impedance for CFL numbers near the maximum prescribed by linear stability analysis.

Results for an isolated electric/magnetic conducting sheet in free-space are presented in Fig. 4 for (a) $(\sigma\, d) = 2.0$ and $(\sigma^* d) = 1.0$ with $\mathcal{A}_1 = 0.4$, and (b) $(\sigma\, d) = 2.0$ and $(\sigma^* d) = 6.0$ with $\mathcal{A}_1 = 0.8$. Results for a material interface with an electric/magnetic conducting sheet are presented in Fig. 5 in which $\varepsilon = 12$ and $\mu = 1.0$ for (a) $(\sigma\, d) = 2.0$ and $(\sigma^* d) = 1.0$ with $\mathcal{A}_1 = 0.5$, and (b) $(\sigma\, d) = 4.0$ and $(\sigma^* d) = 2.0$ with $\mathcal{A}_1 = 0.5$. The specific material properties have been chosen so that the transmission coefficient is positive in (a) and negative in (b) for

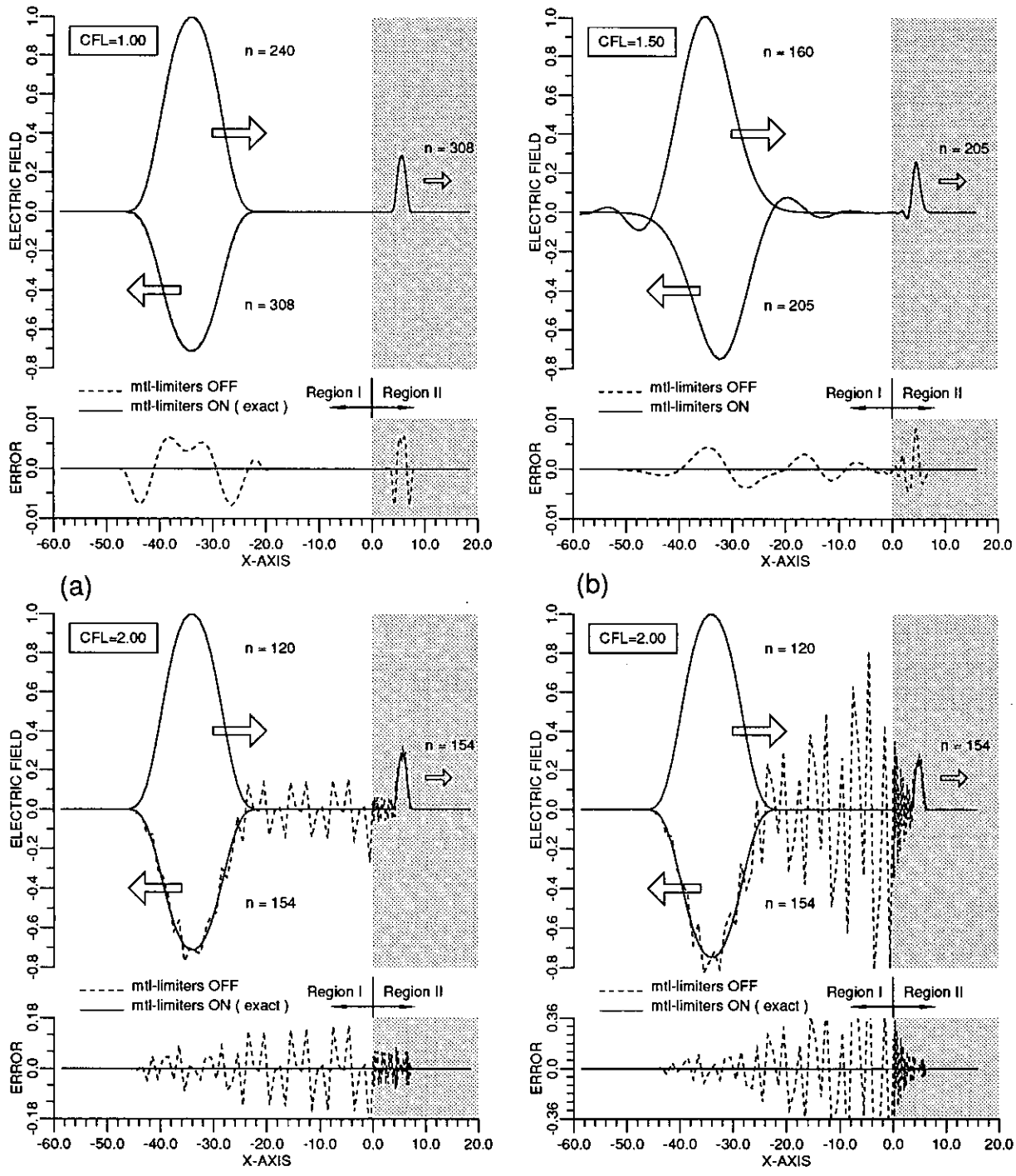

FIG. 2. Analysis of numerical wave propagation across a material interface with no conducting sheet; predictor–corrector scheme with and without material-based limiters. Material properties in region-II: (a) $\varepsilon = 36.0$ and $\mu = 1.0$ at CFL = 1.0, 2.0; (b) $\varepsilon = 49.0$ and $\mu = 1.0$ at CFL = 1.5, 2.0.

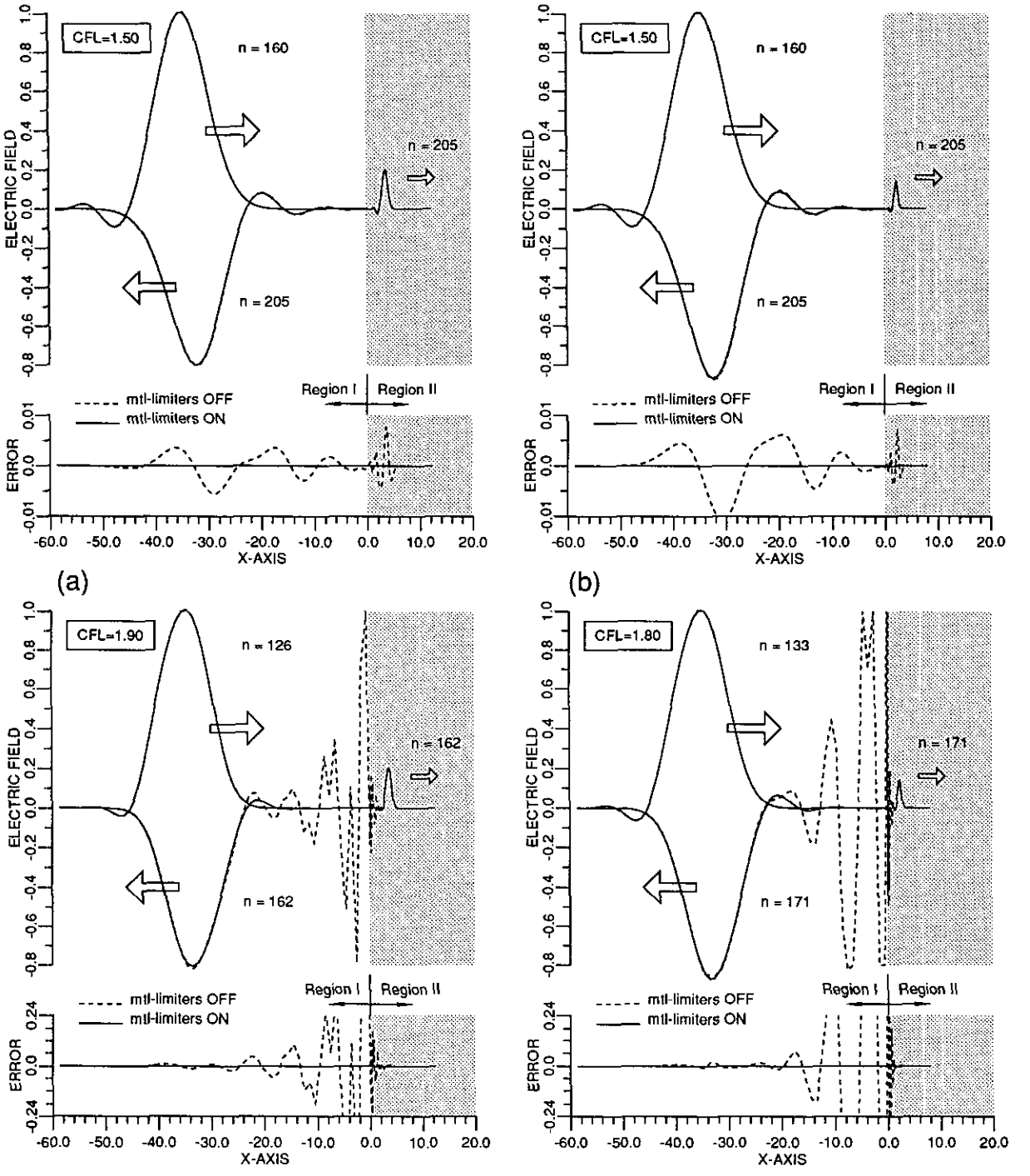

FIG. 3. Analysis of numerical wave propagation across a material interface with no conducting sheet; predictor–corrector scheme with and without material-based limiters. Material properties in region-II: (a) $\varepsilon = 81.0$ and $\mu = 1.0$ at CFL = 1.5, 1.9; (b) $\varepsilon = 196.0$ and $\mu = 1.0$ at CFL = 1.5, 1.8.

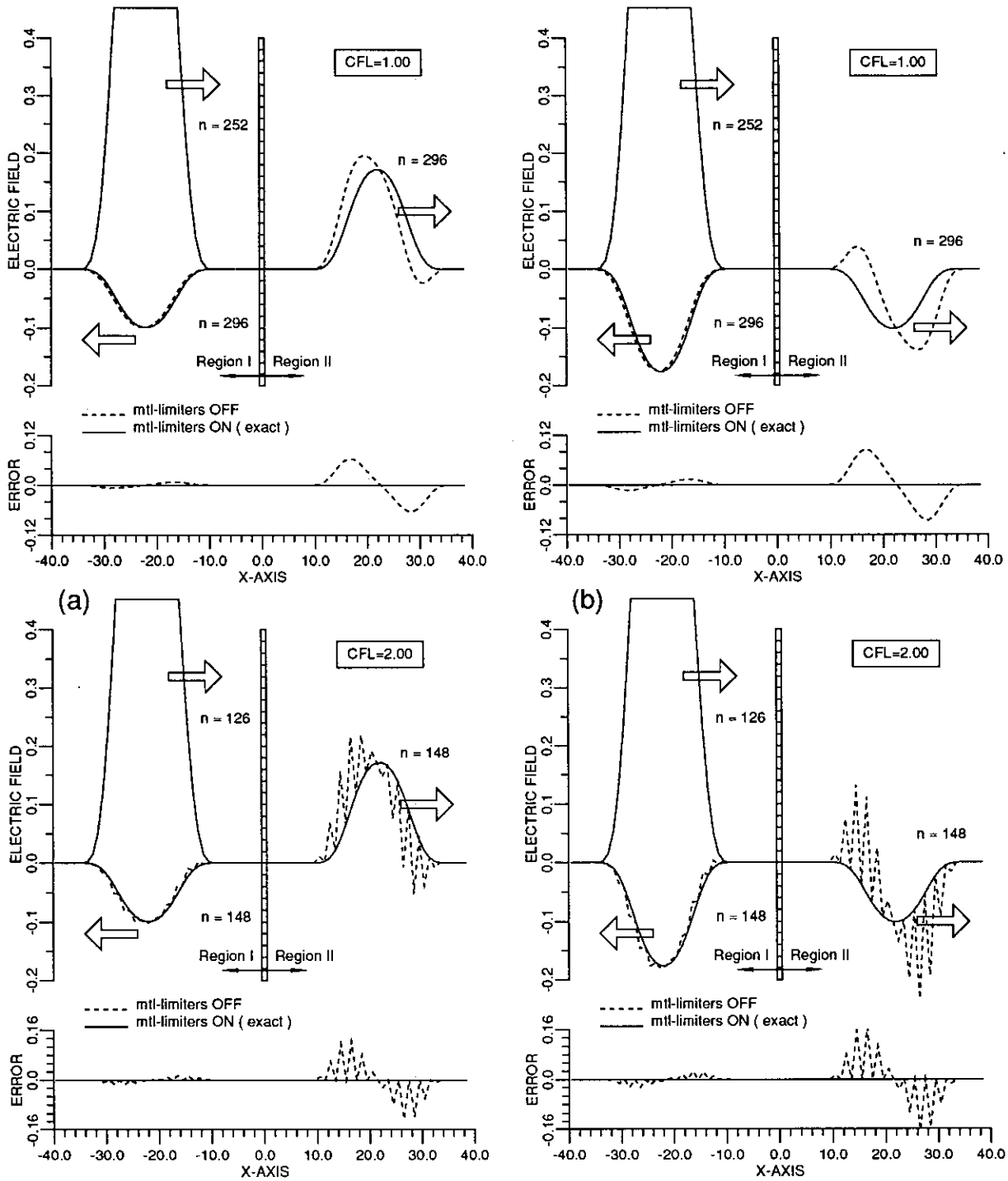

FIG. 4. Analysis of numerical wave propagation across a thin conducting sheet with no material interface; predictor–corrector scheme at CFL = 1.0 and CFL = 2.0 with and without material-based limiters. Properties in region-II: $\varepsilon = 1.0$ and $\mu = 1.0$. Properties of the conducting sheet: (a) $(\sigma\, d) = 2.0$ and $(\sigma^* d) = 1.0$ with $\mathcal{A}_1 = 0.4$; (b) $(\sigma\, d) = 2.0$ and $(\sigma^* d) = 6.0$ with $\mathcal{A}_1 = 0.8$.

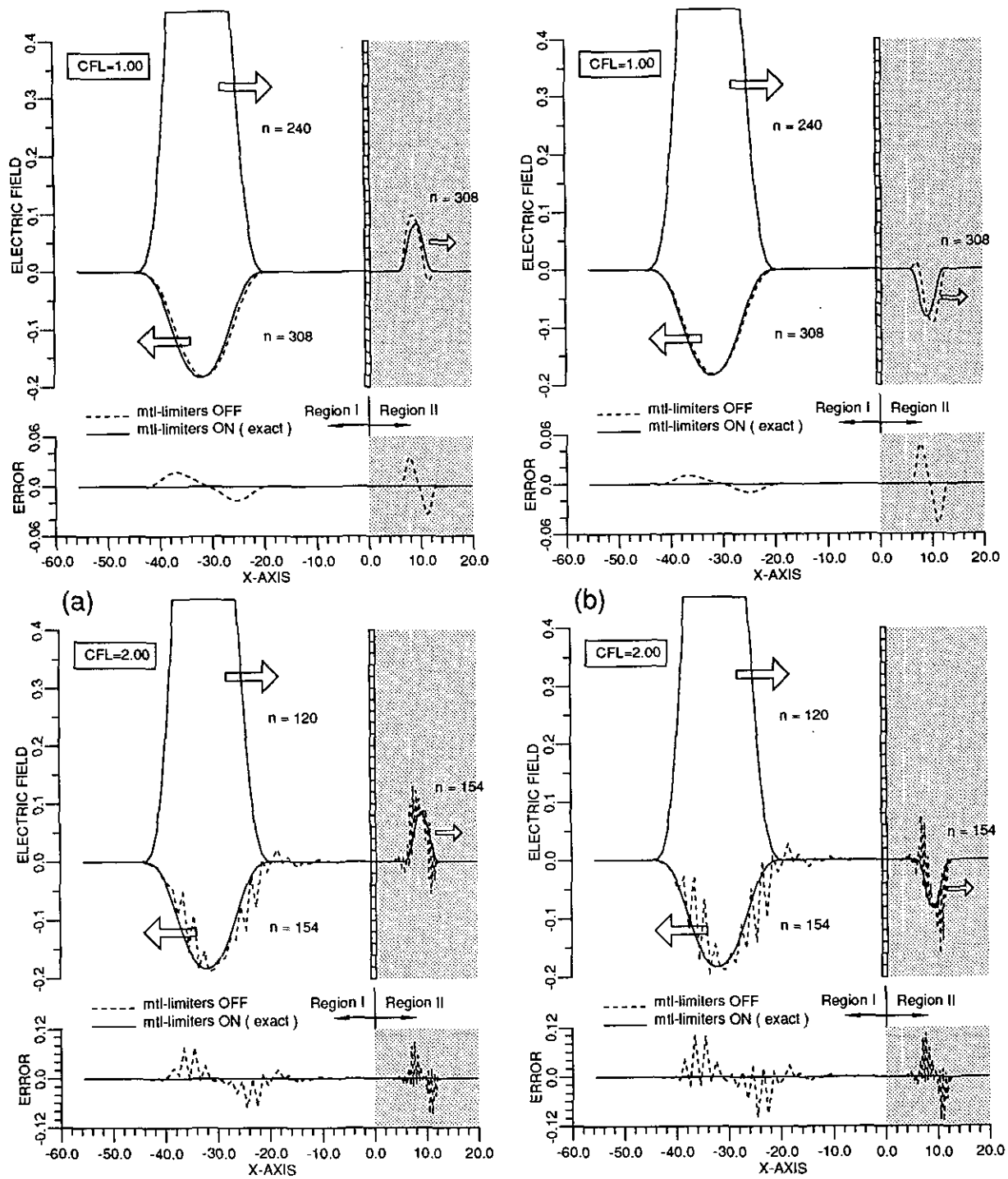

FIG. 5. Analysis of numerical wave propagation across a material interface with a thin conducting sheet; predictor–corrector scheme at CFL = 1.0 and CFL = 2.0 with and without material-based limiters. Properties in region-II: $\varepsilon = 12.0$ and $\mu = 1.0$. Properties of the conducting sheet: (a) $(\sigma d) = 2.0$ and $(\sigma^* d) = 1.0$ with $\mathcal{M}_1 = 0.5$; (b) $(\sigma d) = 4.0$ and $(\sigma^* d) = 2.0$ with $\mathcal{M}_1 = 0.5$.

these geometries. The specific material properties of the conducting sheet cause a large percentage of the incident wave to be absorbed. Results are shown for CFL = 1.0 and CFL = 2.0, to demonstrate that the wave oscillations/distortions still exist. Solution for noninteger CFL number can be computed that are similar to those shown in Fig. 2 and Fig. 3.

The results shown in Fig. 2 through Fig. 5 clearly demonstrate that without material-based limiters the reflected and transmitted waves are distorted as the result of numerically induced oscillations generated at the cell interface. The magnitude of the oscillations are greater than the numerical dispersion for a relatively large discontinuity in the material impedance, for timesteps approaching the maximum CFL number that maintains stability. These oscillations are the direct result of not properly accounting for the wave reflection and transmission on the second-order correction terms in the predictor–correction sequence. The intensity of the oscillations is greater at CFL = 2 than at CFL = 1, and it increases in magnitude as the discontinuity in the material impedance is increased and the number of points per wavelength are decreased. These oscillations can be suppressed by using a larger number of points per wavelength to accurately compute the wave propagation in a body with dielectric material or thin conducting coatings. With material-based limiters, the numerical solution can be obtained at the maximum CFL number prescribed by linear stability analysis, and a smaller number of points per wavelength is required to obtain accurate results.

CONCLUDING REMARKS

With the total-field form of the Maxwell equations, the numerical flux and material-based limiters have been reformulated to include a thin electric concluding sheet and a thin magnetic conducting sheet at the cell interface. Numerical results have confirmed that the upwind predictor–corrector scheme satisfies the one-dimensional perfect-shift condition when material-based limiters are implemented. The material-based limiters correct a deficiency in the upwind predictor–corrector scheme for the solution of the Maxwell equations in nonhomogeneous materials with a spatially varying material impedance and-or thin conducting sheets. The effect of material-based limiters is to improve the solution quality for the reflection and transmission of time-varying electromagnetic fields in nonhomogeneous materials that have relatively large discontinuities in the material impedance. The implementation can reduce the required number of points per wavelength and allow solutions to be obtained at the maximum timestep prescribed by linear stability analysis. These benefits become increasingly important for large realistic configurations in two and three dimensions, given the speed and memory limitations of current computers.

REFERENCES

1. V. Shankar, W. F. Hall, and A. H. Mohammadian, *Proc. IEEE* **77**(5), 709 (1989).
2. V. Shankar, W. F. Hall, and A. H. Mohammadian, AIAA Paper 89-1987CP, 1989 (unpublished).
3. V. Shankar, W. F. Hall, and A. H. Mohammadian, *IEEE Trans. Magn.* **25**(4), 3098 (1989).
4. V. Shankar, W. F. Hall, and A. H. Mohammadian, AIAA Paper 90-3055CP, 1989 (unpublished).
5. V. Shankar, C. Rowell, W. F. Hall, A. H. Mohammadian, M. Schuh, and K. Taylor, *Comput. Systems Eng.* **3**(1–4), 139 (1992).
6. R. F. Warming and R. M. Beam, *AIAA J.* **14,** 1241 (1976).
7. P. Lax, *Hyperbolic Systems of Conservation Laws and the Mathematical Theory of Shock Waves* (SIAM, Philadelphia, 1973).
8. S. Osher and F. Solomon, *Math. Comput.* **38,** 335 (1982).
9. D. G. Bishop and D. A. Anderson, AIAA Paper 92-0456, 1992 (unpublished).
10. D. M. Cook, *The Theory of the Electromagnetic Field* (Prentice-Hall, Englewood Cliffs, NJ, 1975).